Contract No.:

This manuscript has been authored by Battelle Savannah River Alliance (BSRA), LLC under Contract No. 89303321CEM000080 with the U.S. Department of Energy (DOE) Office of Environmental Management (EM).

Submitted to EFM SI on Fracture for Pressure Vessel and Piping

Constraint-Dependent CTOA Determination for Stable Ductile Crack Growth

Xian-Kui Zhu
Materials Technology
Savannah River National Laboratory
Aiken, SC 29808, USA

Poh-Sang Lam
Independent Consultant
Martinez, Georgia 30907, USA

Yuh J. Chao
Department of Mechanical Engineering
University of South Carolina
Columbia, SC 29208, USA

ABSTRACT

The crack tip opening angle (CTOA) has been used as a reliable fracture toughness to characterize stable crack growth for thin-wall structures in low-constraint conditions. Recently, it is found that CTOA can also be utilized as a robust fracture parameter to describe the arrest fracture toughness for gas transmission pipelines in ductile steels. For better understanding the concept of CTOA, this paper presents a brief review on the CTOA definitions and its test methods. And then, four CTOA models are developed for determining the CTOA toughness using conventional single edge notched bend (SENB) specimens, including the load-displacement linear fit model, the logarithmic load-displacement linear fit model, the stable tearing energy model, and the J-differentiation model. Fracture test data from SENB specimens in A285 carbon steel are employed to evaluate the proposed CTOA models. The results show that these CTOA models can determine either identical or comparable critical CTOA values for stable ductile crack growth using the SENB specimens. A constraint-corrected CTOA resistance curve and a constraint-corrected critical CTOA equation are also obtained for A285 carbon steel.

Keywords: CTOA, CTOD, LLD, CMOD, J-integral, J-R curve

1. Introduction

Fracture mechanics methods have been extensively applied to the structural design, crack assessment, and asset integrity management of important infrastructures in the energy industry, including various pressure vessels, storage tanks and oil/gas transmission pipelines. Many pressure vessels are made from stainless steels, whereas pipelines are made from carbon steels. For these ductile steels, the elastic-plastic fracture mechanics methods are often used for engineering critical analysis (ECA), with fracture toughness being characterized by one of three fracture mechanics parameters, i.e., the J-integral, crack tip opening displacement (CTOD), and crack tip opening angle (CTOA), where the J-integral was proposed by Rice [1] in 1968, CTOD was proposed by Well [2] in 1963 and CTOA was proposed by Anderson [3] in 1973. Originally, the J-integral was used to describe the intensity of singularity of the crack-tip field, CTOD was utilized to describe the capability of crack opening, and CTOA was introduced for simulating stable crack growth by finite element analysis (FEA). Nowadays, these fracture parameters have also been used to characterize fracture toughness or resistance of ductile steels against stable crack growth. Over one half of the century, numerous experimental and evaluation methods of fracture toughness have

been proposed for metallic materials. On this basis, different fracture toughness test standard methods have been developed and standardized worldwide. Zhu and Joyce [4] delivered a comprehensive technical review on fracture toughness test standard methods developed by American Society for Testing and Materials (ASTM) for standard fracture specimens with high fracture constraint levels. Zhu [5] presented a technical review on fracture toughness test methods proposed for non-standard fracture specimens with low fracture constraint levels. Newman et al. [6] conducted a technical review on the CTOA/CTOD testing and fracture criteria. In particular, ASTM E1820 [7] was developed for both the initiation toughness and the resistance curve testing with standard specimens under the plane strain conditions in terms of the J-integral or CTOD. ASTM E2472 [8] was developed for the CTOD and CTOA testing for thin-wall compact tension (CT) and middle-crack tension (MT) specimens in the low constraint conditions. More recently, ASTM E3039 [9] was developed for the critical CTOA testing with drop weight tear test (DWTT) specimens for pipeline steels.

It is well known that the J-integral is an energy-based physics parameter, whereas CTOD and CTOA are two directly measurable geometrical parameters. While the J-integral is typically inferred from the applied work done on the specimen from a measured load-displacement curve, CTOD and CTOA can be directly measured on the specimen surfaces during loading. So far, the J-integral has been obtained the most extensive applications in the pressure vessel industry [4], and the geometrical parameters have been obtained more attentions in the pipeline industry [5], where CTOD is used for the strain-based design, and CTOA is used for ductile dynamic fracture control [10-12]. For a gas pipeline in high pressure, fracture initiation is usually followed by extended running crack propagation [10]. This occurs when the driving force caused by internal pressure overcomes the crack propagation resistance of the pipeline steel. It is desired to design a gas pipeline with self-arrest toughness sufficiently high so a running fracture can be avoided or confined within a small portion of the pipe. Recently, many researchers [13-16] investigated the CTOA fracture criterion and measured the critical CTOA value for using as dynamic fracture toughness to arrest a fracture propagation in gas pipelines and demonstrated that the constant CTOA value may serve as an effective fracture toughness to assess the fracture arrest condition to stop a stable fracture propagation over a long distance in a gas pipeline. The recent review on the CTOA testing and applications by Tyson et al. [12] showed that the critical constant CTOA is a promising fracture toughness parameter and the most suited for characterizing fracture resistance against stable crack growth. Therefore, this paper focuses on the CTOA experimental determination and the constraint effect on the critical CTOA toughness during stable ductile crack growth.

The early CTOA testing mainly used thin-wall specimens with surface measurement technologies, such as optical microscopy [17], digital image correction [18], microtopography [19] and others [6]. On this basis, ASTM E2472 was developed in 2006 for CTOA measurement on the surfaces of thin-wall CT or MT specimens using the optical or image technology. However, this standard is not applicable to thick-wall specimens because the direct surface measurement of CTOA may be significantly different from its value at the midplane. To overcome this limitation, Martinelli and Venzi [20] proposed an estimate model to evaluate CTOA from the post-peak absorbed energy using load-displacement data from SENB specimens. Xu et al. [21] modified that model as a simplified single specimen method for more accurate calculation of CTOA from the

load-displacement data in a DWTT test. Subsequently, a number of experimental and numerical investigations [22-26] were performed to determine a constant CTOA during stable crack growth in DWTT specimens using the load-displacement data. On this basis, ASTM E3039 [9] was developed in 2016 for experimental determination of CTOA for ferritic steels at the mid-plane of DWTT specimens, where the specimen thickness is suggested as 6 mm to 20 mm, and is allowed for a thick wall up to 32 mm. Such CTOA toughness has been successfully applied to determine the arrest fracture toughness for stopping dynamic fracture propagation in gas pipelines [14-16]. However, this CTOA test method has a major limitation because the DWTT specimen has a fixed wall thickness W of 76 mm and a fixed initial crack length a of 10 mm, leading to a shallow crack of a/W=0.132. As a result, the effect of crack length or crack-tip constraint becomes a major concern on the critical CTOA value measured using ASTM E3039.

As shown in the review of the CTOD fracture criteria [6, 12], all experimental and numerical data for aluminum alloys and carbon steels demonstrated that the CTOA values are initially high, but progressively decrease to nearly constant values after several millimeters of crack growth. The constant values of CTOA imply that the CTOA fracture criterion is capable of predicting ductile fracture failure of a pressure vessel or pipeline containing a crack. Because the crack-tip constraint level significantly affects the J-integral resistance curve for ductile steels [27-28], it is naturally expected that the constraint may have a similar effect on the constant CTOA toughness during stable crack growth. So far, this important topic only has a limited study in the open literature. Using three-dimensional FEA calculations, Dawicke et al. [29] studied the constraint effects on CTOA during stable tearing in a thin-sheet specimen, and Lam et al. [30] simulated CTOA and its constraint effect for A285 SENB specimens. These authors concluded that CTOA is essentially a function of crack-tip constraint, but the functional dependence between CTOA and a constraint parameter such as A_2 [27-28] has not been established. This motivates the present study.

This paper first presents a brief technical review on the concept of CTOA, its test standard methods, and the commonly used test methods in evaluating a constant CTOA. After that, three load-displacement based models and a J-differentiation model are proposed for determining a constant CTOA over stable crack tearing. A set of fracture test data obtained from SENB specimens in A285 carbon steel with different crack lengths are then used to evaluate those four different CTOA models. The results show that the proposed CTOA models can determine either identical or comparable constant CTOA values over stable crack growth. Based on this, a constraint-corrected CTOA resistance curve and a constraint-corrected critical CTOA equation are obtained for A285 steel.

2. CTOA Definition and Measurement

2.1 CTOA definition

CTOA is referred to as the angle between two crack faces of a growing crack starting from the crack tip. Due to large blunting at the crack tip, the crack faces become curved rather than straight during deformation. Accordingly, the CTOA is simply defined as an angle, ψ, that corresponds to the total CTOD (δ) at a distance d from the crack tip in the order of 1 mm, see Fig. 1. From this figure, CTOA or ψ is calculated by:

$$\psi = 2arctan\left(\frac{\delta}{2d}\right) \quad (1)$$

If ψ is less than 20° degrees, Eq. (1) can be approximated as ψ = δ/d with an error less than 1%.

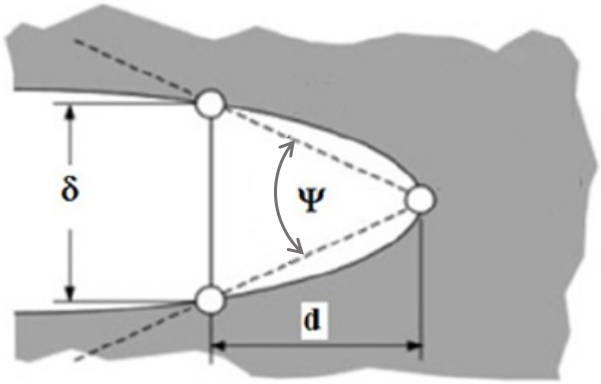

Fig. 1. Definition of CTOA on the curved crack profile.

In experimental measurements, in order to overcome the zigzag pattern of real crack faces, it is more convenient to determine CTOA at several distinct complementary positions (d = 0.5 – 1.5 mm) behind the crack tip. With the CTOD values at the selected positions, an averaged CTOA value should be determined for each loading as an engineering measure.

2.2 Direct surface measurement method in ASTM E2472

In 2006, ASTM published the standard CTOA test method E2472 [8] for measuring the fracture resistance to stable crack extension in metallic materials for thin-wall specimens (both crack length and ligament size are larger than wall thickness with a factor of 4, i.e., a/B ≥ 4 and b/B ≥ 4) under the low-constraint conditions. This standard determines a critical constant value of CTOA over stable crack tearing on CT and MT specimens subject to bending or tensile loading. Both thin-sheet CT and MT specimens require anti-buckling guides during fracture testing. Direct surface measurements of CTOA are recommended as standard methods in E2472, and the critical CTOA is an average of values determined from Eq. (1) using the four-point approach within the minimum and maximum crack extensions. Two techniques recommended for the direct surface measurement of CTOA during stable crack tearing are optical microscopy (OM) [17] and digital image correlation (DIC) [18]. Both techniques produce nearly identical CTOA results. As pointed out by Newman et al. [6], these direct surface measurement methods of CTOA have been extensively used in the aerospace industry for testing aluminum alloy sheet specimens.

The direct surface measurement methods were also extended to the determination of CTOA toughness for pipeline steels using other thin-wall bending specimens, including modified double cantilever beam [MDCB] specimen [31-32], modified compact tension (MCT) specimen [33], and DWTT specimen [34]. In comparison to CT and MT specimens, MDCB, MCT, and DWTT specimens provide a longer uncracked ligament to allow a longer stable crack extension in tension. Through comparisons of direct surface measurements of CTOA using MDCB and DWTT specimens, Xu et al. [34] concluded that DWTT specimens are suitable for a mill test because of

its relatively simple specimen design, while MDCB are more suitable for a laboratory test in supporting the DWTT CTOA test.

2.3 CTOA Measurement method in ASTM E3039

Because the pipeline industry favors the DWTT CTOA testing, ASTM developed another standard test method E3039 [9] in 2016 for measurement of the critical CTOA toughness using DWTT specimens for pipeline steels based on the simplified single specimen method proposed by Xu et al. [21]. This method is essentially the same as the single specimen CTOA method proposed by Martinelli and Venzi [20], but with a different calculation procedure. The critical CTOA is defined as the value at the middle thickness of DWTT specimens and is calculated by:

$$CTOA_{\frac{B}{2}} = \frac{8r_p}{\xi}\frac{180}{\pi}\ (degree) \tag{2}$$

where r_p is the rotation factor and ξ is the absolute value of the slope of $\ln(P/P_m)$ versus $(\Delta-\Delta_m)/S$ curve. In which, P_m is the maximum applied force, and Δ_m is the corresponding load-line displacement (LLD). The DWTT specimen is a three-point bend geometry with the crack length a = 10 mm, the width W = 76 mm, thickness B = 6 – 20 mm and can be thick up to 32 mm, and the span S = 254 mm. Note that the rotation factor is an approximate constant of 0.55, but more accurately it is a function of specimen thickness, yield strength and Charpy impact energy [9]. Many experiments showed that the CTOA values derived from applied load-LLD data are in good agreement with the values of $CTOA_{B/2}$ that is measured at mid-thickness of the DWTT specimen. This $CTOA_{B/2}$ is different from CTOAc in ASTM E2472 that is measured and calculated at 1 mm behind the current crack tip on the specimen surface.

2.4 Numerical simulations of CTOA

Extensive elastic-plastic FEA simulations were performed to calculate CTOA for different materials in 2D and 3D conditions [30, 37, 38]. A more detailed review was conducted by Tyson et al. [12]. The FEA simulations were used to determine more accurate CTOA values during stable tearing of cracks for the fracture specimens such as CT, SENB, MT, MCT, MDCB and DWTT. This can facilitate to develop experimental measurement methods of CTOA toughness testing and the determination of crack driving force in terms of CTOA for a real crack. Once the critical CTOA toughness and the CTOA crack driving force are obtained, the stability of crack can be assessed using the following CTOA fracture criterion. The crack is assumed to be safe if the crack driving CTOA is less than the critical CTOA value (ψ_c) for the material during crack extension:

$$CTOA < \psi_c \tag{3}$$

Note that the current work only focuses on determination of the critical CTOA toughness and will not study the CTOA as a crack driving force.

Both available experimental and numerical results showed that CTOA is always very large at crack initiation, and then gradually reduces to a constant value at stable crack tearing, as illustrated

in Fig. 2. During crack growth in a stable manner, the CTOA remains constant and its constant value ψ_c is considered as a characteristic of the fracture resistance of the material.

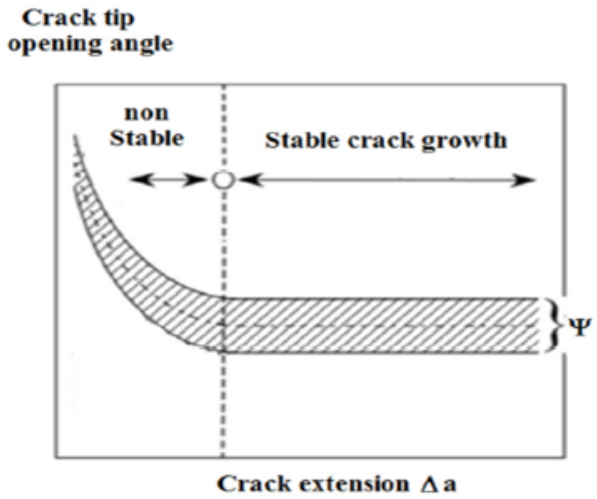

Fig. 2. Evolution of CTOA with scatter during crack extension

3. Indirect CTOA Methods

In this section four indirect models are proposed for inferring the critical CTOA from the conventional fracture testing on SENB specimens, including load-displacement model, logarithmic load-displacement model, stable tearing energy model and J-integral differentiation model.

3.1 Plastic hinge model and load-displacement method

Martinelli and Venzi [20] first proposed a geometrical model to calculate CTOA from the post-peak absorbed energy using load-displacement data for SENB specimens. Because the post-peak energy contains a large portion of plastic deformation energy in the tail of the load-displacement curve, CTOA was overestimated. By removing the tail energy, Xu et al. [21] obtained a modified load-displacement model using a linear curve fit of logarithmic load-displacement data for more accurately determining CTOA for DWTT specimens. On this basis, ASTM E3039 [9] was developed for the determination of CTOA toughness against stable crack tearing using DWTT.

Similarly, the current work adopts the plastic hinge model that was used by BS 7448 [39] in the determination of CTOD for both stationary and growing cracks to derive three load-displacement models for evaluating CTOA from the load-displacement data for SENB specimens. This plastic hinge model assumes that the two arms or halves of the SENB specimen rigidly rotate around a plastic hinge point on the ligament of the specimen in a fracture toughness test for elastic-plastic materials. Figure 3 illustrates the plastic hinge model of SENB specimen for a growing crack, where a small crack extension, da, is generated by a small LLD increment, dΔ. Correspondingly, each half of the specimen rotates a small angle, dθ, which results in a small CTOD increment, dδ, at the crack tip. The distance from the crack tip to the rotation center is assumed to be $r_p b$, where $b = W-a$ is the ligament size and r_p is the plastic rotation factor. For

standard SENB specimens, r_p=0.44 [4]. For other SENB specimens, r_p may depend on the crack size and the strain hardening rate of steels.

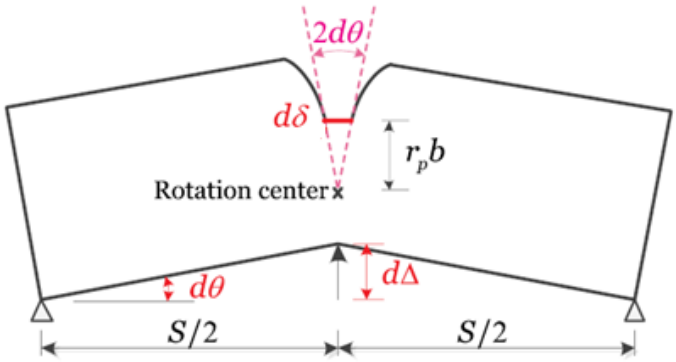

Fig. 3. Plastic hinge model

The rigid plastic model implies that the material is perfectly plastic. For an SENB specimen at the post yield stage, the applied load can be approximated by the limit load for the perfectly plastic material:

$$P = \frac{\lambda \sigma_f B (W-a)^2}{S} \tag{4}$$

where λ is a dimensionless parameter, σ_f is the flow stress that is the average of yield strength and ultimate tensile strength, B is the specimen thickness, W is the specimen width, a is the crack length and S is the span of the beam. It is noted that λ=1.455 for SENB specimens in the perfectly plastic material under the plane strain conditions. For a strain hardening material, however, λ may depend on the loading level and the strain hardening rate of the material. In a fracture test, both applied load and crack length are measured, thus λ can be determined from Eq. (4).

During crack growth, a small LLD increment dΔ generates a small crack extension da and a small CTOD increment dδ. From Fig. 3, the following geometrical relations are obtained:

$$d\theta = \frac{d\Delta}{S/2} \tag{5}$$

$$d\delta = 2 r_p b d\theta \tag{6}$$

where θ is the rotation angle of specimen arms, and r_p is the plastic rotation factor.

When the crack grows a small extension da, CTOD increases a small amount of dδ that corresponds to CTOA at the current crack tip. This can be illustrated by Fig. 1, where d is replaced by da and δ is replaced by dδ. Therefore, similar to the engineering definition of CTOA, Eq. (1) can be written as:

$$\tan\left(\frac{\psi}{2}\right) = \frac{d\delta}{2da} \tag{7}$$

By substituting Eqs (5) and (6) into Eq. (7), one obtains:

$$\tan\left(\frac{\psi}{2}\right) = \frac{2r_p b}{S}\frac{d\Delta}{da} \tag{8}$$

Differentiation of Eq. (4) yields the following differential load:

$$dP = -\frac{2\lambda\sigma_f B b}{S}da \tag{9}$$

From Eqs (8) and (9), CTOA is obtained as a function of P and the slope of the load-LLD curve:

$$\tan\left(\frac{\psi}{2}\right) = -\frac{4r_p P}{S}\frac{d\Delta}{dP} \tag{10}$$

where $\tan(\psi/2) \approx \psi/2$ when $\psi \leq 20^o$ with an error of less than 1%.

Assuming a stable crack growth to take place from crack length a_1 to a_2 after the peak load, CTOA becomes a constant as the critical value (ψ_c). In this case, from Eq. (10), three load-displacement based models are derived next.

- P-LLD linear fit model

Consider two loading points: Point 1 (P_1, Δ_1) and Point 2 (P_2, Δ_2) that are associated with the two crack lengths a_1 and a_2, respectively. Assume there is a linear portion of measured P-LLD data between Point 1 and Point 2. The linear P-LLD data can be best curve-fitted as:

$$P = k\Delta + c \tag{11}$$

Where k and c are two curve fit constants, where k is the slope, and c is the intercept.

Substituting Eq. (11) into Eq. (10) obtains:

$$\tan\left(\frac{\psi_c}{2}\right) = -\frac{4r_p}{S}\left(\Delta + \frac{c}{k}\right) \tag{12}$$

- Ln(P)-LLD linear fit model

Denote the maximum loading point (P_{max}, Δ_{max}). Equation (10) can be rewritten as:

$$\tan\left(\frac{\psi_c}{2}\right) = -4r_p\frac{d(\Delta-\Delta_{max})/S}{d\left(Ln\left(\frac{P}{Pmax}\right)\right)} \tag{13}$$

Using a linear fit for the linear portion of logarithmic load-LLD data, the equation above can be used to determine ψ_c. If $\psi_c \leq 20^o$, Eq. (13) is the same as Eq. (2) that is used by ASTM E3039.

- Stable tearing energy model

Integration of Eq. (10) from Point 1 to Point 2 obtains a third expression of constant ψ_c:

$$\tan\left(\frac{\psi_c}{2}\right) = -\frac{4r_p}{S}\frac{U_2-U_1}{P_2-P_1} \tag{14}$$

where U denotes the external work done on the specimen, and U_2-U_1 is the absorbed stable tearing energy on the stable crack growth. Note that Eq. (14) is the same as Eq. (13) when the linear fit of

Ln(P)-LLD data is used. As a result, the stable tearing energy model is equivalent to the Ln(P)-LLD linear fit model. All three load-displacement models only need the parameter r_P, but not λ.

3.2 J-differentiation model

Since a J-integral resistance curve is determined from measured load, displacement and crack size data for a growing crack, a potential relationship may exist between the J-integral and CTOA over the stable crack tearing. To explore this, considering the η equation that has been used for the experimental estimate of J-integral for a stationary crack [5]:

$$J = \frac{\eta A}{Bb} \tag{15}$$

where η is an LLD-based geometrical factor and is a function of a/W for a specific specimen geometry, and A is the applied external work defined under the P-LLD curve.

For a quasi-steadily growing crack, the complete differential of the J-integral is obtained from the J-integral equation in Eq. (15) [40]:

$$dJ = \frac{\eta}{Bb} P d\Delta - \gamma \frac{J}{b} da \tag{16}$$

where γ is another geometrical factor that is determined by the η factor: $\gamma = \eta - 1 - \frac{b}{W}\frac{1}{\eta}\frac{\partial \eta}{\partial (a/W)}$.

From the differential equation of J-integral in Eq. (16), the slope of LLD-a curve is obtained:

$$\frac{\eta P}{Bb}\frac{d\Delta}{da} = \frac{dJ}{da} + \frac{\gamma}{b} J \tag{17}$$

Substitution of Eq. (17) into Eq. (8) leads to the following expression for CTOA:

$$\tan\left(\frac{\psi}{2}\right) = \frac{2r_p}{\eta \lambda \sigma_f}\left(\frac{dJ}{da} + \frac{\gamma}{b} J\right) \tag{18}$$

For standard SENB specimens, it is often taken that η=2 and γ=1. Note that no assumption of constant CTOA was made in the derivation of Eq. (18). Thus, the J-differentiation equation should be applicable to any crack growth once the fully-plastic condition is reached.

In addition, the CTOD can be converted from the J-integral as used by ASTM E1820 [20] in the form of $\delta = J/(m\sigma_f)$, where the m factor is a weak function of a/W and strain hardening rate of the material. A mathematical definition of CTOA was given by Lam et al. [30]:

$$CTOA = \frac{\partial \delta}{\partial a} \approx \frac{1}{m\sigma_f}\frac{\partial J}{\partial a} \tag{19}$$

Apparently, the mathematical CTOA in Eq. (19) is different from and smaller than the geometrical CTOA in Eq. (18) because the crack growth correction is not considered in Eq. (19) for the mathematical definition of CTOA.

4. Experiment and Results

4.1 Material and specimen geometry

A set of SENB specimens [27, 30] was designed and tested at room temperature based on the guidelines in ASTM E1820 [7], except for the initial crack lengths that were varied to achieve different a_0/W or different levels of crack tip constraint. These specimens were machined from A285 carbon steel Grade C, heat E400 plate with 0.18 wt.% carbon, 0.43 wt.% manganese, and 0.026 wt.% sulfur. The tensile test shows that the 0.2% offset yield stress (Y or σ_0) is 251 MPa (36.4 ksi) and the ultimate tensile stress (T) is 415 MPa (60.2 ksi), leading to Y/T=0.605 (or strain hardening exponent N=5) and the flow stress (σ_f) = 333 MPa (48.3 ksi). In addition, the Young's modulus (E) is 207 GPa (30,000 ksi), and the Poisson ratio is 0.3. Figure 4 shows the true stress–true strain curve for A285 carbon steel. The Y/T ratio indicates that A285 carbon steel is a high strain hardening material.

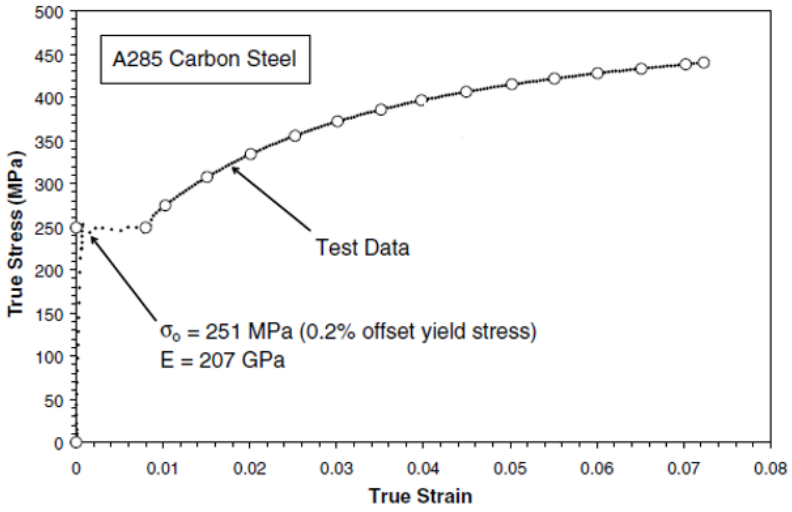

Fig. 4. True stress-strain curve for A285 carbon steel.

The SENB specimen width *W* is 31.75 mm (1.25 in.), the thickness *B* is 15.875 mm (0.625 in.) with a 10% side groove on each side (net thickness BN is 12.7 mm or 0.5 in.), the length *L* is 142.88 mm (5.625 in.), and the span *S* is 127 mm (5 in.). Constant displacement cycles were used to pre-crack the SENB specimen with electric discharge machined (EDM) crack and Chevron notch to create a natural sharp crack tip. The measured fatigue load ranges were 200–3940, 280–1940, 360–3320, and 330–930 N for Specimens 1D, 2C, 2A, and 4C, respectively. The corresponding three-point bending fatigue loads (P_f) defined by ASTM E 1820 are 12,130, 17,610, 4370, and 2130 N, respectively, for these specimens. Since the actual fatigue loads were much lower than P_f, it is expected that the fatigue pre-cracking would not impact the results of the fracture toughness testing. Note that P_f is defined as $0.5B(W - a_0)^2\sigma_f/S^*$ (Eq. (A1.1) in ASTM E 1820), in which the span (S*) in pre-cracking was 101.6 mm (4 in.) and was different from the span used in fracture toughness tests (127 mm or 5 in.). After fatigue pre-cracking, the initial crack

depth to the width ratios (a_0/W) for the fracture toughness test specimens are, respectively, 0.320 (Specimen 1D), 0.350 (Specimen 2C), 0.592 (Specimen 2A), and 0.715 (Specimen 4C).

4.2 Experimental results

The fracture tests on these SENB specimens were originally used to develop a constraint-modified J–R curve for A285 carbon steel storage tanks [27-28]. The same set of test data was used in the study of CTOD/CTOA during crack extension [30]. Due to the large deformation which occurred during testing and the measurement range limitation of the clip gages on hands at the test time, the crack opening mouth clip gauge was not installed. However, the load (or force) and the load-point displacement (i.e., LLD) were measured and are available for data analysis. After the tests were completed, all specimens were heat tinted and then broken in liquid nitrogen. The final crack lengths were measured and determined with a digital image tool which is consistent with the nine-point average approach used by ASTM E1820. The crack lengths during crack growth were measured using the potential drop (PD) technique and were correlated with the actual measurements on the fracture surfaces of the specimens. Figure 5 shows the typical fracture surface of these SENB specimens (in this case, a_0/W = 0.592). It is observed from this figure that a slightly reversed thumbnail crack front was formed because of the presence of side grooves, but a nearly straight line was formed along the crack front. This indicates that the plane strain crack growth conditions were achieved at the crack tips in the specimens.

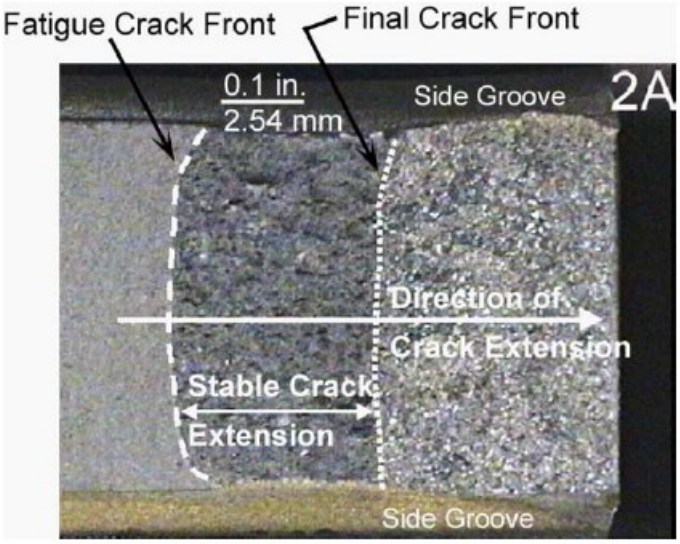

Fig. 5. Typical fracture surface of A285 SENB specimens.

Figure 6 shows the experimental raw data of force versus LLD for three A285 SENB specimens with a_0/W = 0.320, 0.592, and 0.715. All three specimens initially experience linear elastic response with linearly increasing force. Then, plastic strain hardening is followed with nonlinearly increasing force up to the peak load. After that, strain softening begins, and the applied force decreases quickly till the specimen failure. The load-bearing capacity of SENB specimens decreases dramatically as the initial crack length increases. It can be seen that the shallow crack

of $a_0/W = 0.320$, the peak load is P_m=25 kN. For the deep crack of $a_0/W = 0.592$, the peak load drops to P_m=9.75 kN. For another deep crack of $a_0/W = 0.715$, the peak load further drops to P_m=4.5 kN.

Figure 7 shows the experimental data of force versus crack extension for these three specimens. Due to strain hardening, large plastic blunting occurs at the crack tip after the material yields until the peak load is reached, where the crack may start to grow. All specimens experience a large portion of quasi-statically steady crack growth, as is evident in Fig. 7, where a linear relation of load versus crack extension occurs after the peak load.

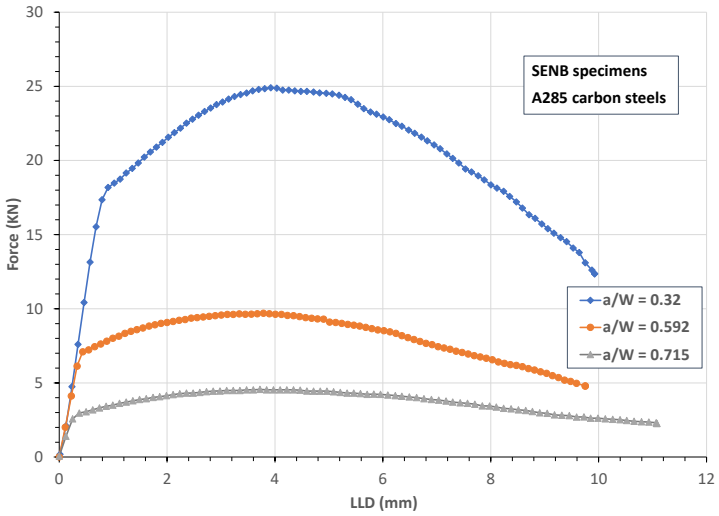

Figure 6. Experimental raw data of force – LLD for three SENB specimens

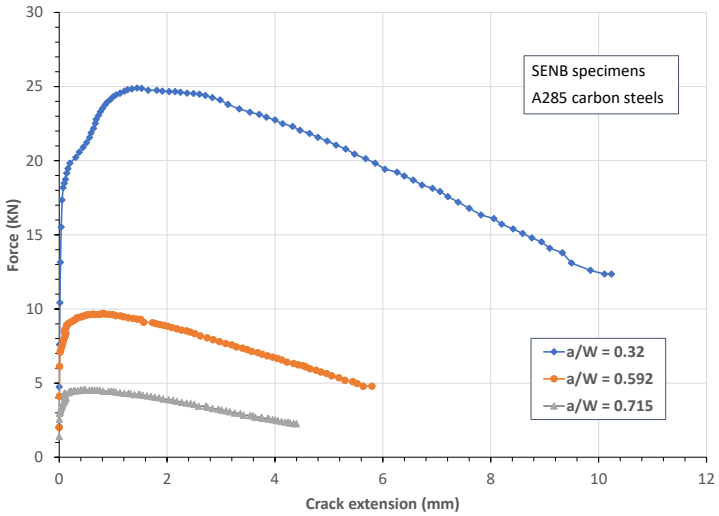

Figure 7. Experimental data of force – crack extension for three SENB specimens

Figure 8 plots the experimental J–R curves [27-28] that were determined using the ASTM E1820 procedures from the load, LLD and crack length as shown in Figs 6 and 7. For completeness, Fig. 8 contains a J–R curve which was subject to cleavage interruption (Specimen 2C) after 1.6 mm of crack extension. In addition, a J–R curve from a standard CT specimen is also

included to compare with those obtained from the SENB specimens. This CT specimen was cut from the same steel plate as the SENB specimens to ensure that identical material source was used, and the only difference is the test specimen design. The width of the CT specimen is 63.58 mm (2.50 in.), and the a/W ratio is 0.47. The specimen height is 48.87 mm (1.92 in.), and its thickness is identical to that of the SENB specimens, that is, 15.875 mm (0.625 in.) with a 10% side groove on each side. Figure 8 clearly shows a distinct specimen size-dependent, in-plane constraint effect on the J-R curves for A285 steel. The current work intends to utilize these experimental data to develop effective estimate methods for the determination of the critical CTOA during stable tearing and quantify the constraint effect on the critical CTOA for A285 steel.

It is noted that, for each specimen, the experiment originally recorded more than one thousand data points from the single specimen test. Without loss of accuracy, only about one hundred data points were extracted evenly over the entire test range and are used for analysis in this work.

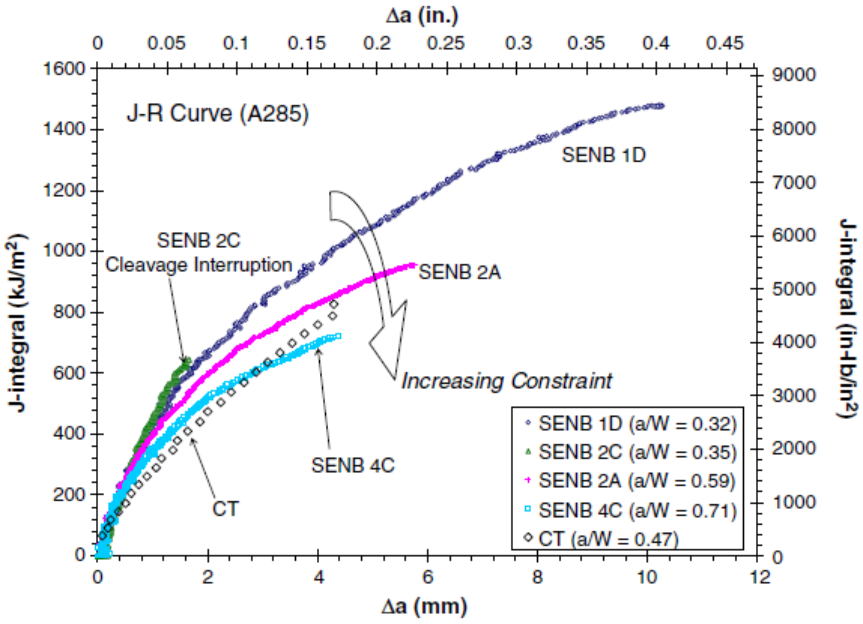

Fig. 8. Experimental J–R curves for various crack length-to-width ratios and two specimen types.

5. Determination of Critical CTOA for A285 steel

5.1 Determination of λ

As evident from Eq. (18), the J-differentiation model requires the value of λ factor for calculating CTOA. From the limit load solution in Eq. (4), the λ factor can be determined from the measured data of applied load and crack size. From the experimental data, the λ factor is calculated for each specimen during the entire deformation. As shown in Fig. 9, the calculated values of λ factor varies from 1 to 2.5. It strongly depends on the deformation level, but weakly depends on the initial crack size (a_0/W). The averaged λ=1.63 over the entire deformation is selected for use hereafter.

Figure 10 compares the measured load P with the limit load solution in Eq. (4) that is normalized with $\sigma_f BW^2/S$ versus the ligament size $(1\text{-}a/W)^2$ during the entire deformation. For each specimen, the normalized load increases from small values in the elastic conditions to the maximum value at the full plastic condition, and then decreases due to crack growth. The limit solution with λ=1.63 seems to be an adequate value to describe the large-scale yielding or fully plastic conditions.

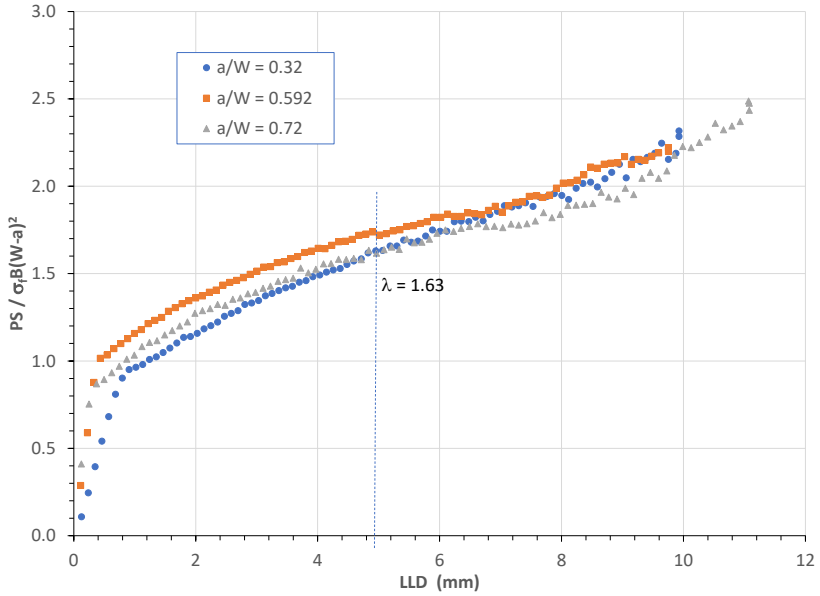

Fig. 9. Variation of λ with LLD for three SENB specimens

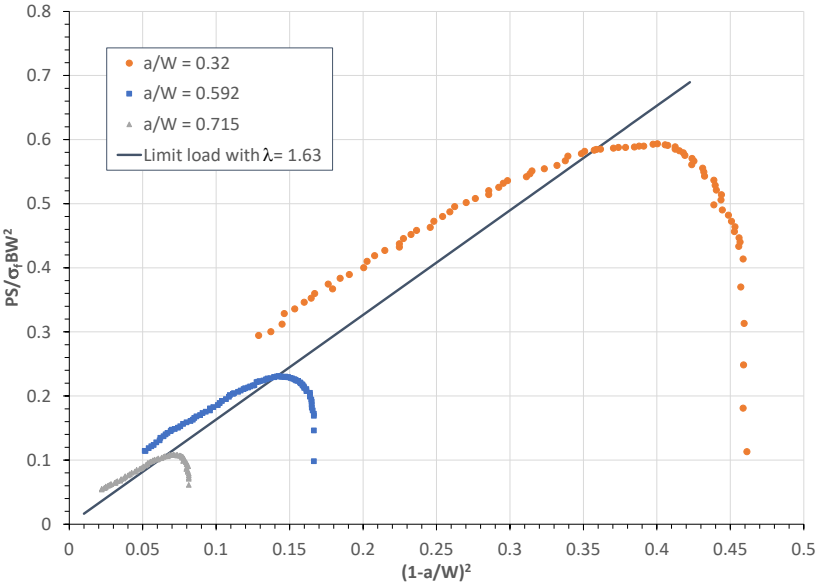

Fig. 10. Comparison of limit load with experimental data for three SENB specimens

5.2 CTOA calculation for SENB with $a_0/W=0.592$

The critical CTOA value is calculated here by using, respectively, the P-LLD linear fit model (Eq.(12)), the Ln(P)-LLD linear fit model (Eq. (13)), and the J-differentiation model (Eq. (18)). It is noted that each model requires a differentiation for calculating CTOA. In general, any experimental raw data contain variations or fluctuations more or less due to test machine vibration and signal noises. Thus, the experimental data need to be smoothened by using a regression method to determine a representative function, from which the derivative can be calculated.

Figure 11 replots the force – LLD curve as shown in Fig. 6 for the deep crack of $a_0/W = 0.592$. The data between the two vertical lines (P/P_{max}=0.86 and 0.63) can be approximated by a linear relation that represents the stable crack growth. The best curve fit equation of the linear P-LLD data is:

$$P = 0.9672\Delta + 14.29 \quad \text{(kN)} \tag{20}$$

Thus the two constants in Eq. (12) are k = 0.9672 kN/mm, and c = 14.29 kN.

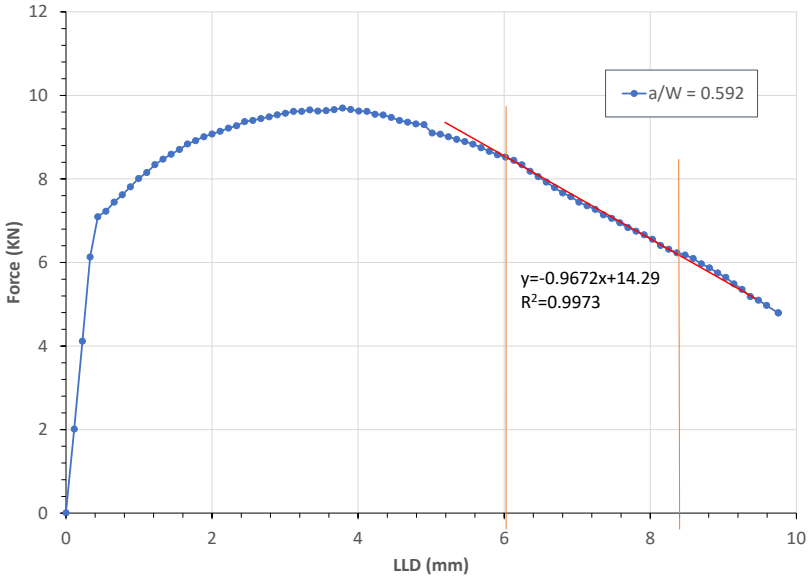

Fig. 11. Experimental Force – LLD data and the linear curve fit

Figure 12 replots the force-LLD data shown in Fig. 11 but with different scales ($a_0/W=0.592$): the y-axis is $Ln(P/P_{max})$ and the x-axis is $(\Delta-\Delta_{max})/S$ for $a_0/W=0.592$, where P_{max} is the maximum or peak load, and Δ_{max} is the LLD at P_{max}. The data between the two red vertical lines can be approximated by a linear relation that represents stable crack growth The best curve fit equation of the linear $Ln(P/P_{max})$ vs $(\Delta-\Delta_{max})/S$ data is:

$$Ln(P/P_{max}) = 17.022(\Delta - \Delta_{max})/S + 0.1623 \tag{21}$$

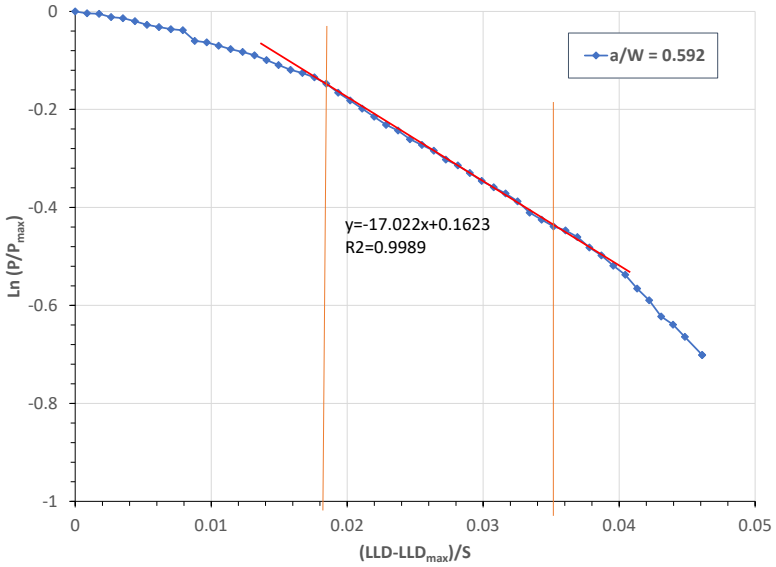

Fig. 12. Experimental $\text{Ln}(P/P_{max})$ versus $(\text{LLD}-\text{LLD}_{max})/S$ data and the linear curve fit

Figure 13 shows the experimental data of entire post-peak force-LLD records for $a_0/W=0.592$. The best curve fit of the P-LLD data is described in the following third-order polynomial form:

$$P = 0.0126\Delta^3 - 0.3112\Delta^2 + 1.5516\Delta + 7.6198 \quad \text{(kN)} \tag{22}$$

This polynomial function of P-LLD data will be used in Eq. (10) to estimate CTOA over the entire range of crack extension to serve as a reference for comparing results obtained by other models.

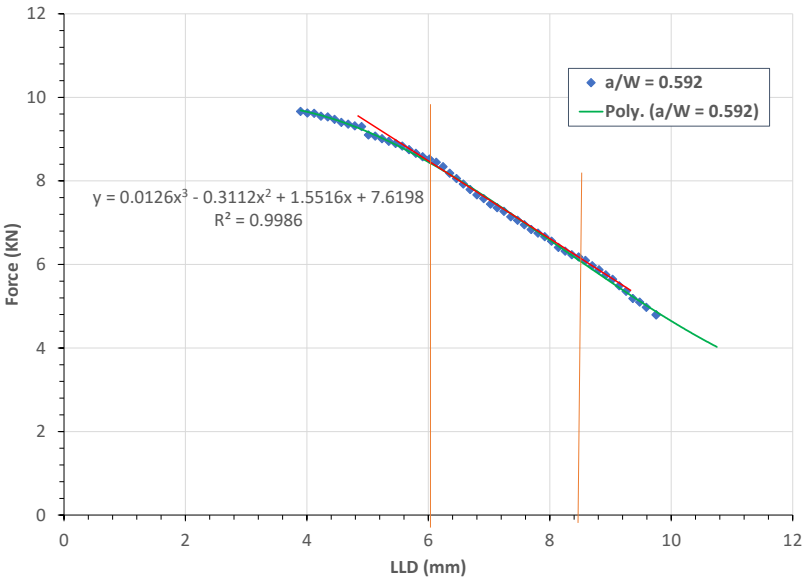

Fig. 13. Experimental data of post-peak force-LLD and its best curve fit

Figure 14 plots the experimental J-R curves obtained by the potential drop (PD) [27] and by the normalization method (NM) [28] for A285 SENB specimen with $a_0/W=0.592$. It is shown that the PD and NM methods determine nearly identical J-R curves. Because a normalization function was used in the NM method, its J-R curve is relatively smooth. In contract to this, the PD method did not use any analytical function, and its J-R data have naturally fluctuations. This paper employs the experimental J-R curve from the PD method for evaluating CTOA. The best curve fit of this J-R curve is described in the following forth-order polynomial:

$$J = -1.4622(\Delta a)^4 + 22.118(\Delta a)^3 - 135.41(\Delta a)^2 + 447.14(\Delta a) - 47.44 \quad (\text{kJ/m}^2) \qquad (23)$$

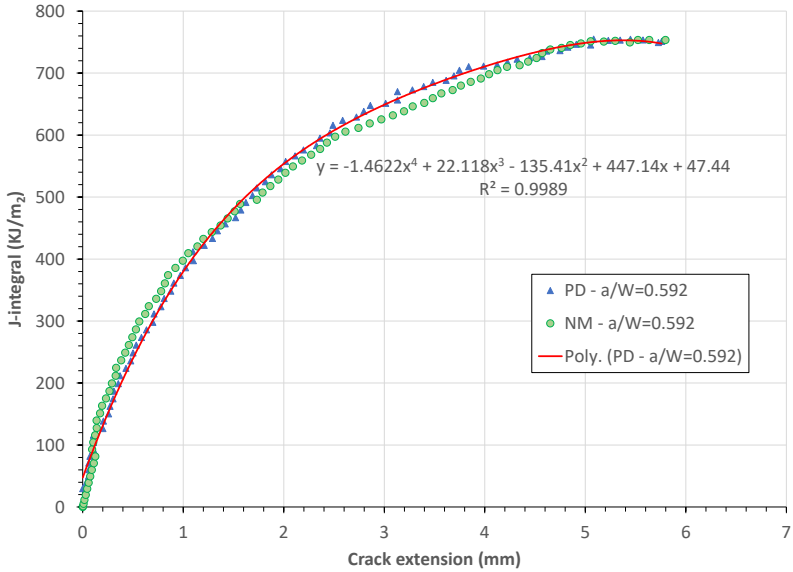

Fig. 14. Experimental J-R curve and its best curve fit

Using the above curve fitted equations, CTOA resistance curves or the critical constant CTOA values can be determined using the load-displacement models and the J-differentiation model. Figure 15 shows the CTOA against crack extension obtained using the P-LLD linear fit, the Ln(P)-LLD linear fit, the J-differentiation method, and the P-LLD polynomial fit, respectively for the SENB specimen with the deep crack of $a_0/W=0.592$. It is demonstrated that all models determine comparable critical CTOA values over the range of stable crack extension from Δa = 2.5 mm to 4.5 mm. It is observed that over the stable crack growth zone: (1) the Ln(P)-LLD linear fit model determines a constant CTOA, $\psi_c = 11.85^o$, (2) the P-LLD linear fit model determines a linearly decreasing CTOA with an average value of $\psi_c = 11.99^o$, (3) the J-differentiation model can determine CTOA over the entire crack growth, and the CTOA curve becomes flat over the stable crack growth zone with an average value of $\psi_c = 12.59^o$, and (4) the J-differentiation model is better than the P-LLD polynomial fit over the entire crack extension.

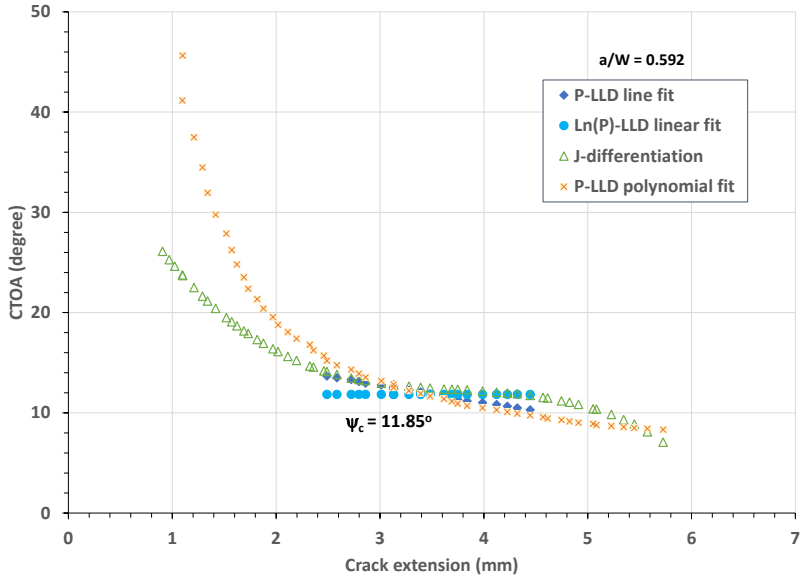

Fig. 15. CTOA toughness against crack growth for SENB specimen with $a_0/W=0.592$

5.3 CTOA calculation for SENB specimen with $a_0/W=0.715$

In the similar manner as used in Section 5.2, four best curve-fitted equations are obtained and used to calculate the CTOA values for the load-displacement models and the J-differentiation model. Figure 16 shows the CTOA against crack extension obtained using the P-LLD linear fit, the Ln(P)-LLD linear fit, the J-differentiation method, and the P-LLD polynomial fit, respectively for the SENB specimen with the deep crack of $a_0/W=0.715$.

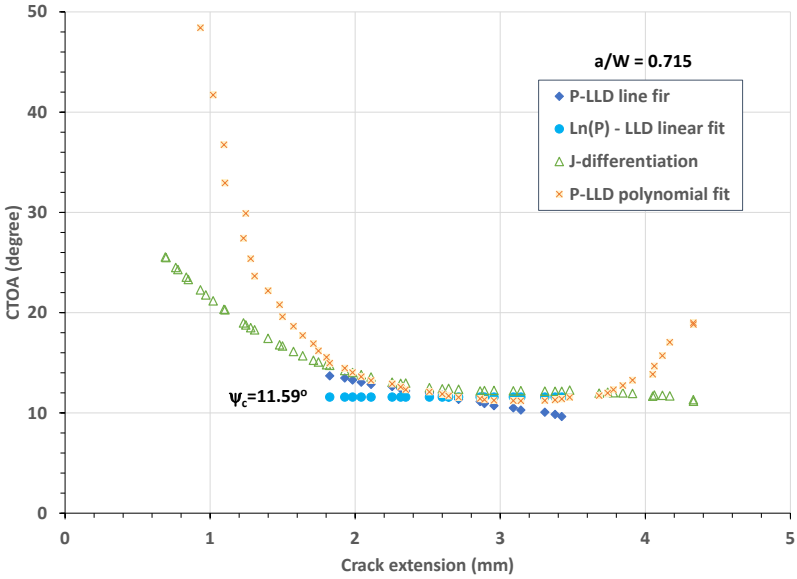

Fig. 16. CTOA toughness against crack growth for SENB specimen with $a_0/W=0.715$

It is demonstrated that all models determine comparable critical CTOA values over the range of stable crack extension from Δa = 1.8 mm to 3.5 mm. Figure 16 shows that over the stable crack growth zone, (1) the Ln(P)-LLD linear fit model determines a constant CTOA, ψ_c = 11.59°, (2) the P-LLD linear fit model determines a linearly decreasing CTOA with an average value of ψ_c = 11.67°, (3) the J-differentiation model can determine CTOA over the entire crack growth, and the CTOA curve becomes flat over the stable crack growth zone with an average value of ψ_c = 12.52°, and (4) the J-differentiation model is better than the P-LLD polynomial fit over the entire crack extension.

5.4 CTOA calculation for SENB specimen with a_0/W=0.320

In the similar manner as used in Section 5.2, four best curve-fitted equations are obtained and used to calculate the CTOA values for the load-displacement models and the J-differentiation model. Figure 17 shows the CTOA against crack extension obtained using the P-LLD linear fit, the Ln(P)-LLD linear fit, the J-differentiation method, and the P-LLD polynomial fit, respectively for the SENB specimen with a_0/W=0.320.

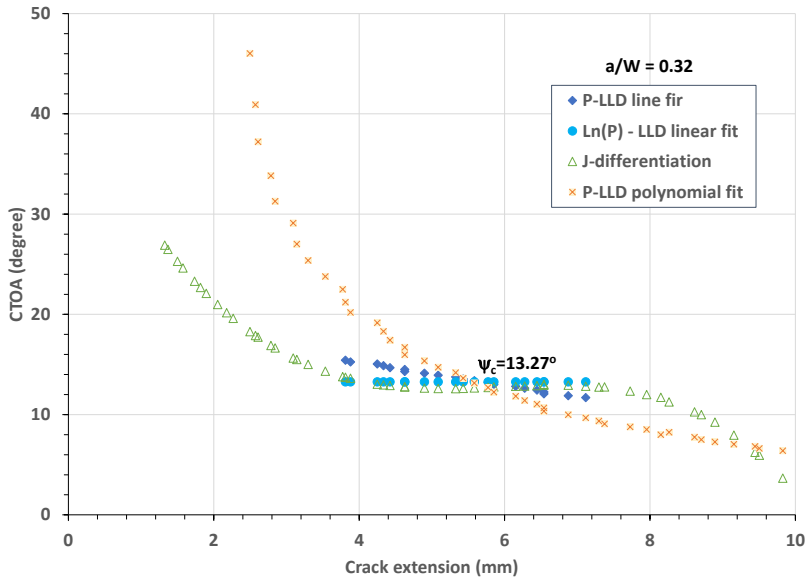

Fig. 17. CTOA toughness against crack growth for SENB specimen with a_0/W=0.320

It is demonstrated that all models determine comparable critical CTOA values over the stable crack extension from Δa = 3.8 mm to 6.5 mm. From Fig. 17, it is observed that over the stable crack growth zone, (1) the Ln(P)-LLD linear fit model determines a constant CTOA, ψ_c = 13.27°, (2) the P-LLD linear fit model determines a linearly decreasing CTOA with an average constant value of ψ_c = 13.38°, (3) the J-differentiation model can determine CTOA over the entire crack growth, and the CTOA curve becomes flat over the stable crack growth zone with an average constant value of ψ_c = 12.88°, and (4) the J-differentiation model is better than the P-LLD polynomial fit over the entire crack extension. In addition, a specimen with a longer ligament (W-a_o) will provide a longer stable crack growth zone and thus determines more accurate CTOA.

5.5 Determination of constraint-corrected CTOA resistance curve

Using the experimental J-R curves from the SENB specimens, Zhu et al. [28] obtained the following constraint-corrected J-R curve for A285 carbon steel:

$$J(\Delta a, A_2) = C_1(A_2)(\Delta a)^{C_2(A_2)} \tag{34}$$

where A_2 is the constraint parameter , and C_1 and C_2 are two constraint-related parameters to characterize the crack resistance J-R curve. For A285 steel, the two parameters were determined from FEA results as $C_1 = -1089A_2 + 25.534;\ C_2 = -0.618A_2 + 0.267$. Figure 18 shows the constraint-corrected J(A_2)-R curves for three SENB specimens. The J-R curves obtained from the experimental PD method are also included in the figure for comparison. It is observed that the constraint-corrected J-R curve is not the same as the curve-fitted results, but is conservative over the range of crack growth for each specimen.

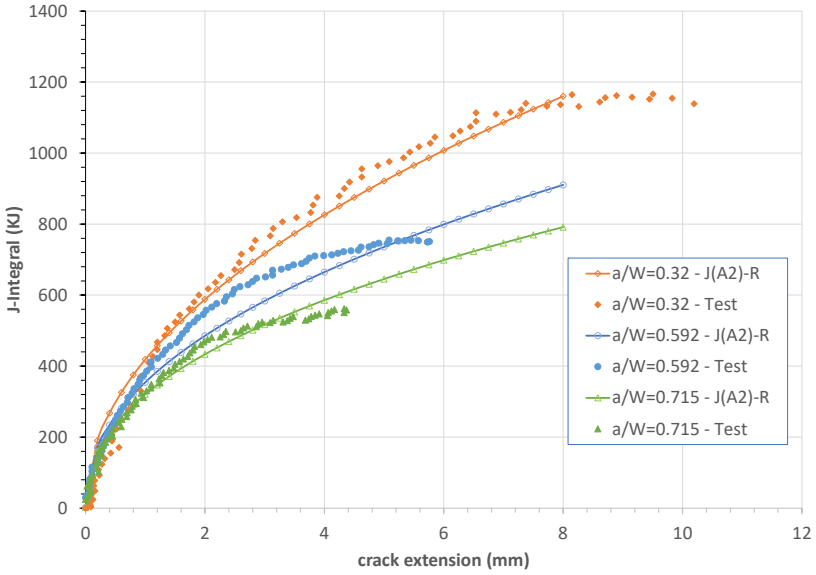

Fig. 18. Experimental and Predicted J-R curves for three SENB specimens

Substitution of Eq. (34) into the J-differentiation Equation (18) obtains:

$$\tan\left(\frac{\psi}{2}\right) = \frac{r_p}{\lambda\sigma_f}\left(\frac{C_2}{\Delta a} + \frac{1}{b_0 - \Delta a}\right) J(\Delta a, A_2) \tag{35}$$

Since the J-integral and the parameter C_2 in the above equation have been obtained, the CTOA in Eq. (35) is known as a function of constraint parameter A_2 and crack extension Δa, as shown in Fig. 19. These curves may be referred to as constraint-corrected CTOA resistance curves. It is seen from Fig. 19 that (1) these curves determine comparable minimum values of CTOA, (2) the flat part for describing stable crack growth becomes short as the initial crack size increases, (3) the shallow crack of $a_0/W = 0.32$ (with the longest ligament for stable crack growth) determines the constant CTOA of $\psi_c = 13.47^o$, and the deepest crack of $a_0/W = 0.715$ determines a slightly larger CTOA. As a result, the constraint level may have limited effect on the critical CTOA. Several

factors may result in this observation, and one of them may be the similar slopes of these constraint-corrected J-R curves. However, the slope of the constraint-corrected J-R curves for the two deep cracks is larger than those from the experimental J-R curves, as shown in Fig. 18. The larger the slope, the larger the CTOA.

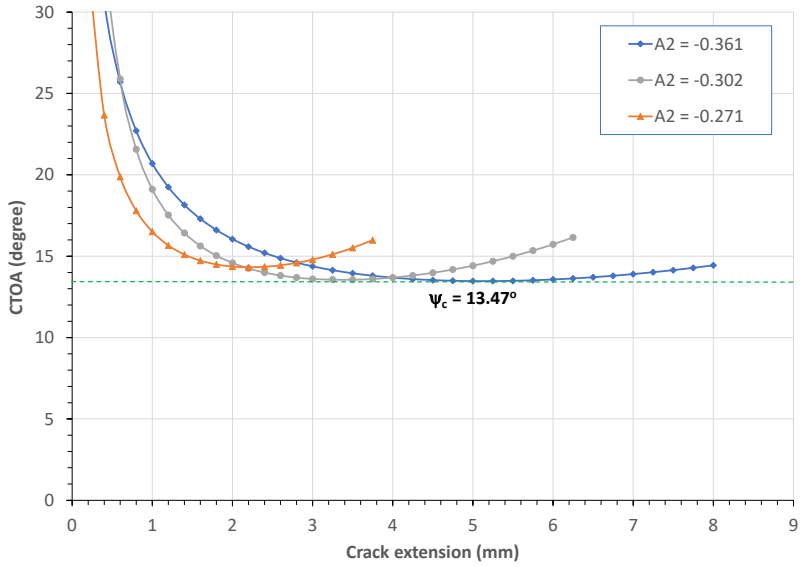

Fig. 19. Constraint-corrected CTOA resistance curves for A285 steel

5.6 Constraint effect on the critical CTOA

Sections 5.2 to 5.5 determine the critical CTOA (ψ_c) for each specimen using different models. Figure 20 compares the critical CTOA values obtained by different models versus the constraint level for each crack, where the constraint parameter was obtained by Zhu et al. [28] as A_2 = -0.361, -0.302, and -0.271, respectiely for a_0/W = 0.32, 0.592, and 0.715. It is seen from Fig. 20 that the constraint level has small effects on the critical CTOA values, as observed for the constraint-corrected CTOA resistance curves shown in Fig. 19. From the FEA numerical simulations, Parmar et al. [41] reported similar observation that the constraint level described by the T-stress has only a small effect on the CTOA for pipeline steels.

For the convience of comparison, take the constant ψ_c results from the Ln(P)-LLD linear fit model as reference values. The linear regression determines the following weak linear relationship between the critical ψ_c and the constraint parameter A_2:

$$\psi_c = -19.337A_2 + 6.215 \quad (degree) \tag{36}$$

This relationship reveals that the critical CTOA slightly decreases with increasing constraint level at the crack tip, which is consistant with experimental observations [6]. For example, the CTOA values measured at the midplane are always smaller than the suface measurements, because the midplane has higher constraint level than the surface. Experiments also showed that the directly

measured CTOA on specimen surface over stable crack tearing descrease with increasing wall thickness, because the constraint level along the crack front increases as the wall becomes thicker.

Comparinig with the reference critical CTOA values, Fig. 20 shows that (1) the critical CTOA values obtained from the P-LLD linear fit model is nearly the same as the reference values, (2) at the low constraint level for the shallow crack, all models determine a consistent critical CTOA value, (3) the J-differentiatioin model with the use of experimental J-R curves determines constraint-independent CTOA values, and (4) the J-differentiatioin model with use of the constraint-corrected J-R curves determine elevated critical CTOA values. Several factors may be involved with this discrepancy, and one of them is the η and γ factors used in Eq. (18). In this paper, η=2 and γ=1 are used. Those values were recommended in the older versions of ASTM E1820 [7], and thus were untilized in the determination of the experiemental J-R curves [27] and constraint-corrected J-R curves [28]. However, the current version of ASTM E1820 suggests more accurate values of these two geometrical factors, that is, η=1.9 and γ=0.9 for standard SENB specimens with deep cracks. If smaller values of the η and γ factors are used, the critical CTOA values for the two deep cracks would drop down somehow to be closer to their respective reference critical CTOA values (the dotted line in Fig. 20).

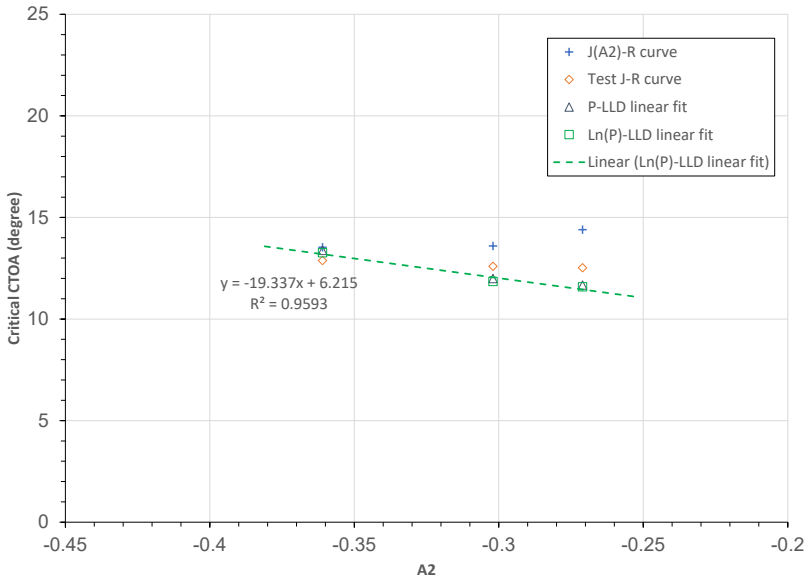

Fig. 20. Correlation between critical CTOA and constraint parameter A_2

6. Conclusions

This paper investigated the evaluation methods for calculating the critical CTOA over stable crack growth and assessing the crack tip constraint effect on the critical CTOA using the conventional SENB specimens. For better understanding the concept of CTOA, a brief review on the CTOA definitions and its test methods were first provided. On this basis, four CTOA models were developed for determining the CTOA toughness using SENB specimens. These include the load-displacement linear fit model, the logarithmic load-displacement linear fit model, the stable tearing energy model, and the J-differentiation model. To evaluate these CTOA models,

experimental data using SENB specimens for A285 carbon steel were employed to calculate the critical CTOA. The results based on different models were compared and analyzed. The following conclusions can be drawn:

1) Using the load-displacement data, the P-LLD linear fit model and the Ln(P)-LLD linear fit model were developed. The former determines a linearly decreasing CTOA, and the latter determines a constant CTOA over stable crack growth. On average, these two models can determine the nearly identical CTOA values.
2) From the concept of absorbed stable tearing energy during stable crack growth, the stable tearing energy model was developed for calculating the constant CTOA. This model is equivalent to the Ln(P)-LLD linear fit model in determination of the critical CTOA.
3) From the differentiation equation of the J-integral for a growing crack, the J-differentiation model was developed for determining CTOA during ductile crack growth. Using experimental J-R curves, the J-differentiation model determined a comparable critical CTOA value over stable crack growth as the load-displacement models. Furthermore, this model also determined a set of CTOA resistance curves over the entire range of crack extension.
4) Using the constraint-corrected J-R curves, the J-differentiation model determined a set of constraint-corrected CTOA resistance curves. However, the resulting critical CTOA values are insensitive to the in-plane constraint level. Further investigation on this topic is needed.
5) A weakly linear constraint corrected CTOA equation was obtained for A285 carbon steel. It can be used for estimating the critical CTOA toughness for crack assessment under different crack tip constraint levels.

ACKNOWLEDGEMENTS

The first author, Xian-Kui Zhu, appreciates the partial support by the Laboratory Directed Research and Development (LDRD) program within the Savannah River National Laboratory (SRNL). This document was prepared in conjunction with work accomplished under Contract No. 89303321CEM000080 with the U.S. Department of Energy (DOE) Office of Environmental Management (EM).

References

[1] Rice JR. A path independent integral and the approximate analysis of strain concentration by notches and cracks. *Journal of Applied Mechanics*, 1968; 35: 379-386.

[2] Wells AA. Application of fracture mechanics at and beyond general yielding. *British Welding Journal*, 1963; 10: 563-570.

[3] Anderson H. A finite element representation of stable crack growth, *Journal of Mechanics and Physics in Solids*. 1973, 21: 337-356.

[4] Zhu XK, Joyce JA. Review of fracture toughness (G, K, J, CTOD, CTOA) testing and standardization. *Engineering Fracture Mechanics*, 2012; 85: 1-46.

[5] Zhu X.K. "Review of Fracture Toughness Test Methods for Ductile Materials in Low-Constraint Conditions," *International Journal of Pressure Vessels and Piping*, Vol. 139-140, 2016: 173-183.

[6] Newman JC, James MA, Zerbst U. A review of the CTOA/CTOD fracture criterion. *Engineering Fracture Mechanics*, 2003; 70: 371-385.
[7] ASTM E1820-20b. *Standard Test Method for Measurement of Fracture Toughness*. American Society of Testing and Materials International, West Conshohocken, PA, 2020.
[8] ASTM E2472-12. *Standard Test Method for Determination of Resistance to Stable Crack Extension under Low-Constraint Conditions*. American Society of Testing and Materials International, West Conshohocken, PA, 2018.
[9] ASTM E3039-20. *Standard Test Method for Determination of Crack Tip Opening Angle of Pipe Steels using DWTT Specimens*. American Society of Testing and Materials International, West Conshohocken, PA, 2020.
[10] Zhu XK. State-of-the-art review of fracture control technology for modern and vintage gas transmission pipelines. *Engineering Fracture Mechanics*, 2015; 148: 260-280.
[11] Horsley DJ. Background to the use of CTOA for prediction of dynamic ductile fracture arrest in pipelines. *Engineering Fracture Mechanics*, 2003; 70: 547-552.
[12] Tyson WR, Newman JC, Xu S. Characterization of stable ductile crack propagation by CTOA: Review of theory and applications. *Fatigue Fract Eng Mater Struct* 2018; 41: 2421-2437.
[13] Benamara M, Pluvinage G, Capelle J, Azari Z. The CTOA as a parameter of resistance to crack extension in pipes under internal pressure. *Lecture Notes in Mechanical Engineering – Fracture at All Scales* (Eds: G Pluvinage, L Milovic), 2017: 59-88.
[14] Amara MB, Pluvinage G, Cappelle J, Azari Z. New numerical tools to calibrate the two curves method using the CTOA criterion. *Engineering Fracture Mechanics*, 2019; 205: 532-546.
[15] Xu S, Bassindale C, Xue J, Williams BW, Wang X. Recent progress in development of ductile fracture arrest methodology based on CTOA: test standard, transferability and methodology. *Proceedings of the 13th International Pipeline Conference*, September 29-30, 2020, Virtual, Online. IPC2020-9299.
[16] Zhen Y, Zu Y, Cao Y and Niu R. Effect of accurate prediction of real-time crack tip position on dynamic crack behaviors in gas pipeline. *Journal of Natural Gas Science and Engineering*, 2021; 94: 104136.
[17] Mahmoud S, Lease K. The effect of specimen thickness on the characterization of critical CTOA in 2024-T351 aluminum alloy. *Engineering Fracture Mechanics*, 2003; 70: 443-456.
[18] Chao YJ, Sutton MA. Accurate measurement of two- and three-dimensional surface deformations for fracture specimens by computer vision. *Experimental Techniques in Fracture* (editor: Epstein JS), VCH Publisher, 1993: 59-94.
[19] Lloyd WR. Microtopography for ductile fracture progress characterization: Part 1 – theory and methodology. *Engineering Fracture Mechanics*, 2003; 70: 387-401.
[20] Martinelli A, Venzi S. Tearing modulus, J-integral, CTOA and crack profile shape obtained from the load-displacement curve only. *Engineering Fracture Mechanics*, 1996; 53: 263-277.
[21] Xu S, Bouchard R, Tyson WR. Simplified single-specimen method for evaluating CTOA, *Engineering Fracture Mechanics*, 2007; 74: 2459-2464.
[22] Xu S, Tyson WR. CTOA measurement of pipe steels using DWTT specimen, *Proceedings of the 7th International Pipeline Conference*, September 29 – October 3, 2008, Calgary, Alberta, Canada. IPC2008-64060.

[23] Xu S, Petri N, Tyson WR. Evaluation of CTOA from load vs load-line displacement for C(T) specimen, *Engineering Fracture Mechanics*, 2009; 76: 2126-2134.
[24] Xu S, Tyson WR, Simha CHM. Testing for resistance to fast ductile fracture: measure of CTOA, *Journal of Pipeline Engineering*, 2013; 12: 165-173.
[25] Fang J, Zhang J, Wang L. Evaluation of cracking behavior and critical CTOA values of pipeline steel from DWTT specimens, *Engineering Fracture Mechanics*, 2014; 124-125: 18-29.
[26] Shuai J, Tu S, Wang J, Ren X, He J, Zhang Z. Determination critical CTOD for energy-load curves with DWTT specimen, *Engineering Fracture Mechanics*, 2017; 186: 47-58.
[27] Lam PS. Chao YJ, Zhu XK, Kim Y, Sindelar TL. Determination of constraint-modified J-R curves for carbon steel tanks. *Journal of Pressure Vessel Technology*, 2003; 125: 136-143.
[28] Zhu XK, Lam PS, Chao YJ. Application of normalization method to fracture resistance testing for storage tank A285 carbon steel. *International Journal of Pressure Vessels and Piping*, 2009; 86: 669-676
[29] Dawicke DS, Neman JC, Bigelow CA. Three-dimensional CTOA and constraint effects during stable tearing in a thin-sheet material, *ASTM STP 1256*, American Society for Testing and Materials, 1995: 223-242.
[30] Lam PS, Kim Y, Chao YJ. The non-constant CTOD/CTOA in stable crack extension under plane strain conditions. *Engineering Fracture Mechanics*, 2006; 73: 1070-1085.
[31] Darcis PP, McCowan CN, Windhoff H, McColskey JD, Siewer TA. Crack tip opening angle optical measurement methods in five pipeline steels. *Engineering Fracture Mechanics*, 2008; 75: 2453-2468.
[32] Amaro RL, Sowards JW, Drexler ES, McColskey JD, McCowan C. CTOA testing of pipeline steels using MSCB specimens. *Journal of Pipeline Integrity*, 2013; 3: 199-215.
[33] Yan D, Shuai J, Wang J, Tu S. A new specimen for high-grade pipeline steels CTOA test. *Engineering Fracture Mechanics*, 2015; 148: 203-212.
[34] Xu S, Tyson WR, Eagleson R. Measurement of CTOA of pipeline steels using MDCB and DWTT specimens. *Proceedings of the 8th International Pipeline Conference*, Sept 27 – Oct 1, 2010, Calgary, Alberta, Canada. IPC2010-31076.
[35] Zhen Y, Li X, Cao Y, Zhang S. A novel method to determine critical CTOA directly by load-displacement curve. *Engineering Fracture Mechanics*, 2020; 230: 107013.
[36] Lu L, Wang S, Tong G. Relationship between incremental J integral and crack tip opening angle in elastic plastic materials. *European Journal of Mechanics / A Solids*, 2019; 75: 399-409.
[37] Gullerud AS, Dodds RH, Hampton RW, Dawicke DS. Three-dimensional modeling of ductile crack growth in thin sheet metals: computational aspects and validation. *Engineering fracture Mechanics*, 1999; 63: 347-374.
[38] Zhen Y, Chang Q, Cao Y, Niu R. A novel unified characterization parameter of in-plane and out-of-plane constraints based on critical CTOA. *Fatigue and Fracture of Engineering Materials and structures*, 2021; 44: 1305-1317.
[39] BS 7448-1. *Fracture Mechanics Toughness Tests – Part 1: Method for Determination of K_{Ic}, Critical CTOD and Critical J Values of Metallic Materials*. British Standards Institution, 1991.

[40] Zhu XK. Improved incremental J-integration equations for determining crack growth resistance curves. *Journal of Pressure Vessel Technology*, 2012; 134: 051404.
[41] Parmar S, Bassindale C, Wang X, Tyson WR, and Xu S. Simulation of ductile fracture in pipeline steels under varying constraint conditions using cohesive zone modeling. *International Journal of Pressure Vessels and Piping*, 2018; 162: 86-97.